LA-UR-18-29064
Approved for public release; distribution is unlimited.

Title: Analysis of 191Ir(n, g) data measured at the DANCE facility

Author(s): Rusev, Gencho Y.

Intended for: Report

Issued: 2018-09-24

Analysis of ^{191}Ir(n,γ) data measured at the DANCE facility

G. Rusev

Nuclear and Radiochemistry Group (C-NR), LANL
(Dated: September 21, 2018)

Measurements of the ^{191}Ir(n,γ) reaction were performed at the DANCE facility in 2013. Description of the data analysis is presented. Deduced relative neutron-capture cross section is reported. The cross section is compared to the ENDF evaluation.

I. OVERVIEW

A campaign for measuring the neutron-capture cross sections of ^{191}Ir and ^{193}Ir was initiated in 2008 at the Detector for Advanced Neutron Capture Experiments (DANCE). A few measurements were performed with $^{\rm nat}$Ir (2008) and thin electroplated ^{193}Ir (2009) and ^{191}Ir (2010) targets revealing the need for use of heavier targets to improve the counting statistics. Samples of stippled isotopically enriched iridium with masses of 16 mg were used during the Los Alamos Neutron Science Center (LANSCE) beam cycles of 2012 and 2013. Results from the analysis of the ^{193}Ir(n,γ) measurement have already been reported in Ref. [1]. In this paper, we report the analysis of the ^{191}Ir(n,γ) data obtained through LANSCE proposal NS-2012-4040-A "Neutron Capture Measurements on ^{191}Ir and ^{193}Ir at DANCE" by C. W. Arnold and co-proposers T. A. Bredeweg, D. J. Vieira, E. M. Bond, M. Jandel, G. Rusev, W. A. Moody, J. L. Ullmann, A. Couture, S. Mosby, J. M. O'Donnell, and R. C. Haight.

In the next section, we will review the ^{191}Ir measurements from 2013 and then will focus on the main components of the data analysis as energy calibration and time alignment of the DANCE detectors (section IV), background reduction (section V), and neutron flux determination (section VI). We will present our results for the relative ^{193}Ir(n,γ) cross section in section VII.

II. ^{191}Ir MEASUREMENTS

The ^{193}Ir(n,γ) measurements were performed with the DANCE array located at flight-path 14 of the Manuel J. Lujan, Jr. Neutron Scattering Center at LANSCE [2]. Spallation neutrons, produced by irradiation of a tungsten target with 800-MeV protons with a repetition rate of 20 Hz, were used in the measurements. At flight-path 14, the low-energy part of the neutron-flux distribution was additionally enhanced by a water-moderator block with a thickness of 2.54 cm (*cf.* section VI). The spallation target is shielded by a 2-m thick concrete wall. The neutrons are collimated to a narrow beam by a double-truncated copper collimator forming a spot at the target position with a full width at the half maximum of 0.7 cm. The collimator consists of four sections with a total length of 3 m. A detailed description of the neutron facility at the Lujan Center and the properties of the beam can be found in Refs. [3, 4].

DANCE is a high-granularity and highly-efficient γ-ray calorimeter consisting of 160 BaF_2 crystals in a 4π geometry. The exact solid angle of DANCE is 3.6π. The initial design of DANCE is described in Ref. [5]. Each BaF_2 crystal has the same volume of 734 cm^2 and length of 15 cm. The DANCE crystals are in four different shapes with the same solid angle and with the same γ-ray detection efficiency. The detectors are wrapped with very thin reflective and light-insulation films to minimize the energy loss when a γ ray scatters from one crystal to another. The total efficiency of DANCE for detection of a γ ray with energy of 1 MeV was simulated to be 86% [6] and confirmed by a measured value of 86.2(17)% [7]. For typical cascades of 3-4 γ rays, the total efficiency is higher than 95% [5, 6].

The BaF_2 crystals were chosen for DANCE detectors, because they are among the fastest scintillation materials with a rise time of 1.5(2) ns [8]. The scintillation light of BaF_2 has a short (τ = 0.8 ns, λ = 220 nm) and a long (τ = 630 ns, λ = 310 nm) component providing pulse-discrimination capabilities.

DANCE is designed to be a γ-ray calorimeter measuring the total γ-ray energy (E_γ^{tot}) released by the (n,γ) reaction. The high granularity of DANCE and the relatively small size of its detectors enable accurate measurement of the individual γ rays, their E_γ spectra and multiplicities of the γ-ray cascades. The high efficiency of the detectors requires only a tiny detector-response correction and, respectively, reduces the systematic uncertainty due to the detector-response simulations. Note, the systematic uncertainty of simulated results is in general not well known. The fast response time of the BaF_2 detectors provides good neutron time-of-flight (TOF) measurement with "start" (T_0) given by the proton bunch shortly before impinging the tungsten neutron-production target and "stop" - the first DANCE detector that registered a γ ray. The TOF in ns is transformed to neutron energy E_n in eV using the relation

$$E_n = \frac{1}{2} m_n V_n^2 = \\ = \frac{1}{2} 1.675 \cdot 10^{-27}\text{kg} \frac{(20.28\text{m})^2}{((TOF + T_{delay})10^{-9}\text{s})^2} \\ \times 6.242 \cdot 10^{18} \frac{\text{eV}}{\text{Joule}}, \quad (1)$$

where m_n and V_n are the mass and velocity of the neutron. The estimated distance of DANCE to the neutron moderator is 20.28 m. T_{delay} is the delay time of the neutron in the moderator. This time depends on E_n, but we will consider it to be a constant $T_{delay} = 523$ ns adjusted to reproduce well the resonance region of the (n, γ) reaction.

For completeness, we will mention a couple drawbacks of DANCE. Worse energy resolution of $\Delta E_\gamma / E_\gamma \approx 15\%$ of the BaF_2 is the trade off for the high γ-ray efficiency and fast timing. Each detector has a given electronics threshold and γ rays with small energies may not be detected. Having relatively small size crystals causes E_γ^{tot} to be incomplete. Compton scattering of a γ ray from one detector to another is the main reason for reducing E_γ^{tot}.

The data acquisition (DAQ) of DANCE [9] is based on Acqiris DC265 digitizers (8-bit resolution, 500 MHz sampling rate). Each digitized card has six input channels. The digitizers operate in a "continuous" mode providing, dead-time free acquisition of the events in a TOF window of 250 μs. To double the length of the TOF window, the signal of each DANCE detector is split and fed into two digitizer cards with different delays for their 250-μs windows relative to T_0. We will refer to the two digitizer cards as Card0 and Card1. The impedance of the two digitizers was different to avoid signal reflection, 50 Ω for the first one (Card0) and 1 MΩ for the second one (Card1). The high impedance of Card1 worsens the performance of the signal processing (*cf.* section IV for details).

Four digitizer cards were installed in a crate with an on-board computer. A front-end program running on the on-board computer did the analysis of the signal waveforms. Each waveform was integrated in a few regions: 100-ns long baseline prior to the signal, 64-ns long fast component, and five sequential regions of 200 ns for the slow component. A MIDAS [10] based program read the data from all 15 on-board computers and saved it to disk. In addition, the 32 samples of the fast component, showing the rise of the signal, were saved to disk for accurate determination of the TOF in offline analysis.

The ^{191}Ir measurements were performed in October 2013 using two iridium targets enriched to ^{191}Ir. An electroplated target with a thickness of 1.22 mg/cm^2 was used to scan the low-energy region below $E_n = 1$ eV. The target consists of deposits with diameter of 0.5 cm on the two sides of a 2.5-μm thick titanium foil. Details on the target preparation can be found in Ref. [11]. A picture of the target is shown in Fig. 1 and a list of the measurements with this target is given in Table I.

The second target has a mass of 16 mg. It was prepared by stippling ^{191}Ir powder on a 7.6-μm thick Kapton tape and sealed by an 1-μm thick Mylar foil. A picture of the target is shown in Fig. 1. This target was used for high-statistics measurement above $E_n = 1$ eV. A list of the measurements is given in Table II.

In addition, a few measurements were performed with standard DANCE targets of ^{208}Pb and ^{197}Au listed in Table III. Details for these targets can be found in Ref. [12]. A list of measurements with standard γ-ray sources for calibration purposes is given in Table IV.

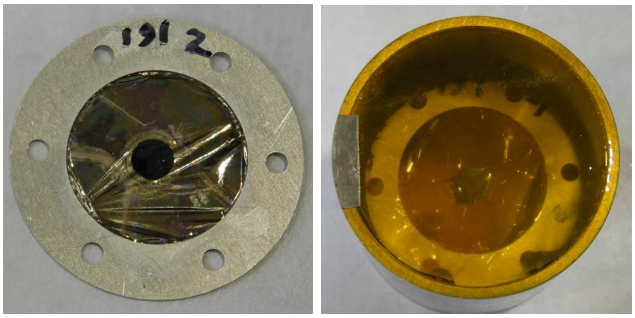

FIG. 1: Picture of the double-sided electroplated ^{191}Ir target (left) with a total thickness of 1.22 mg/cm^2 and a picture of the 16-mg target (right) of ^{191}Ir powder stippled to a Kapton tape and sealed with a Mylar foil.

First run	Last run	Delays	Neutron fluence
43619	43634	(-10, 240)	$79.69(14)\times10^9$
43635	43636	(-10, 480)	$5.91(4)\times10^9$
43637	43638	(480, -10)	$5.24(4)\times10^9$
43639	43640	(-10, 720)	$6.47(4)\times10^9$
43641	43642	(720, -10)	$6.25(4)\times10^9$
43643	43643	(-10, 960)	$2.41(2)\times10^9$
43644	43644	(960, -10)	$3.62(3)\times10^9$
43645	43645	(1200, -10)	$2.08(2)\times10^9$
43646	43646	(1200, 1440)	$5.45(4)\times10^9$
43647	43647	(1680, 1920)	$2.60(3)\times10^9$
43648	43651	(240, -10)	$21.13(7)\times10^9$
43652	43652	(2160, 2400)	$2.39(3)\times10^9$
43653	43653	(2640, 2880)	$2.14(2)\times10^9$
43654	43658	(240, -10)	$32.65(9)\times10^9$
43659	43660	(3120, 3360)	$3.55(3)\times10^9$
43661	43661	(3600, 3840)	$0.981(17)\times10^9$
43662	43662	(5000, 9150)	$2.51(2)\times10^9$
43663	43663	(4080, 4320)	$2.99(3)\times10^9$
43664	43664	(7000, 7240)	$0.857(15)\times10^9$

TABLE I: List of the run numbers, delays (Card0, Card1) and the neutron fluence (cf. section VI) from the ^{6}Li monitor for the measurements with the electroplated 1.22-mg/cm^2 thick ^{191}Ir target.

III. DATA PROCESSING

The recorded data files contain a lot of lengthy information like waveforms and MIDAS headers. Replaying the raw data files slows down the analysis. Therefore, we considered a two-stage analysis. At the first stage we determine the detector ID from the MIDAS header by mapping the number of the crate, digitizer card in the crate and the input channel of the card. Because each DANCE detector is read by two individual digitizers (Card0 and Card1), we offset the detector IDs from

First run	Last run	Delays	Neutron fluence
43835	43849	(-10, 240)	$29.43(9)\times10^9$
43850	43876	(240, -10)	$52.36(12)\times10^9$
43878	43895	(-10, 240)	$34.70(10)\times10^9$
43896	43905	(-10, 480)	$15.65(6)\times10^9$
43906	43912	(-10, 720)	$16.98(7)\times10^9$
43913	43915	(-10, 960)	$6.55(4)\times10^9$
43916	43918	(-10, 9150)	$4.57(3)\times10^9$
43919	43934	(-10, 200)	$33.76(9)\times10^9$
44012	44214	(-10, 240)	$368.4(3)\times10^9$

TABLE II: Measurements with the 16 mg ^{191}Ir target.

First run	Last run	Delays	Neutron fluence
^{208}Pb, mass 30 mg			
44215	44282	(-10, 240)	$159.1(2)\times10^9$
44284	44284	(0, 240)	$0.045(3)\times10^9$
44285	44286	(-10, 240)	$1.65(2)\times10^9$
^{197}Au, thickness 10^3Å, diameter 7 mm			
43612	43614	(-10, 550)	$12.52(5)\times10^9$
^{197}Au, thickness 10^3Å, diameter 4 mm			
43615	43618	(-10, 550)	$17.84(7)\times10^9$

TABLE III: Measurements with ^{208}Pb and ^{197}Au targets.

Card1 by 200 in order to keep them separated. Thus we double the number of detectors, but this discrimination is necessary, because the signals from Card1 have poorer quality than the same ones from Card0. We obtain more accurate TOF from the recorded waveform using a software leading-edge discriminator. We correct the waveform integral corresponding to the fast component of the light emission of the BaF_2 crystal for the baseline and label it as I_{fast}. We add up the five integrals of the slow component and also correct for the baseline and define it as I_{slow}. At the end, we order in time all events according to their TOF and save to disk only four numbers for each γ-ray event: detector ID, TOF, I_{fast}, and I_{slow}. The new data files are about 10% smaller than the original MIDAS files. The first-stage analysis was performed using the code FARE [13] with small modifications.

The new data files are processed by a program that applies energy calibration to all detectors and performs time alignment of the detectors described in section IV. The code also applies cuts to remove events from α particles and re-triggering explained in section V. At the final step, the analysis code creates coincidence events of γ rays detected within a 10-ns wide coincidence window and fills histograms of interest.

Source	First run	Last run	Delays
^{22}Na	43935	43969	(0, 250)
^{137}Cs	43970	43972	(0, 250)
^{54}Mn + ^{133}Ba	43973	43977	(0, 250)
^{133}Ba	43978	43979	(0, 250)
^{60}Co	43989	43996	(0, 250)
^{60}Co	43997	43999	(0, 0)
^{60}Co + ^{137}Cs	44000	44002	(0, 250)
^{88}Y	44003	44011	(0, 250)

TABLE IV: Measurements with standard γ-ray sources.

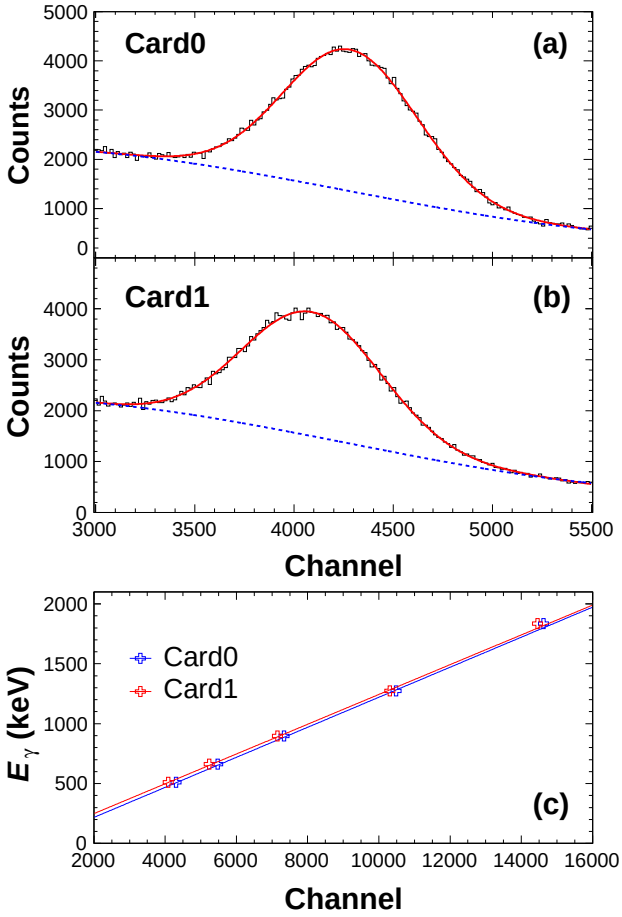

FIG. 2: Peaks from the 0.511 MeV γ rays measured with detector 0 and digitizer cards 0 (a) and 1 (b). The peaks are fitted with a Gaussian function (red) superimposed on a background (dashed blue). Lineal fit of the energy calibration for the same detector is shown in the bottom panel (c).

IV. DETECTOR CALIBRATION

The energy calibration of the DANCE detectors was obtained from the measurements with standard γ-ray sources ^{22}Na, ^{137}Cs, and ^{88}Y (*cf.* Table IV). Initially, the signals from the α particles have to be removed (*cf.* section V), because they contaminate the γ-ray spectra with a few strong peaks. To reduce the background due to Compton scattering and pair creation, we required no other DANCE detector to fire within 10 ns after a γ ray was registered in one of the detectors. We collected γ-ray spectra for each DANCE detector (2×160, because of having two digitizers per detector) for each of the source measurements. We fit the five γ-ray peaks (0.511, 0.662, 0.898, 1.275, and 1.836 MeV) individually using a Gaussian function with a background. The background was

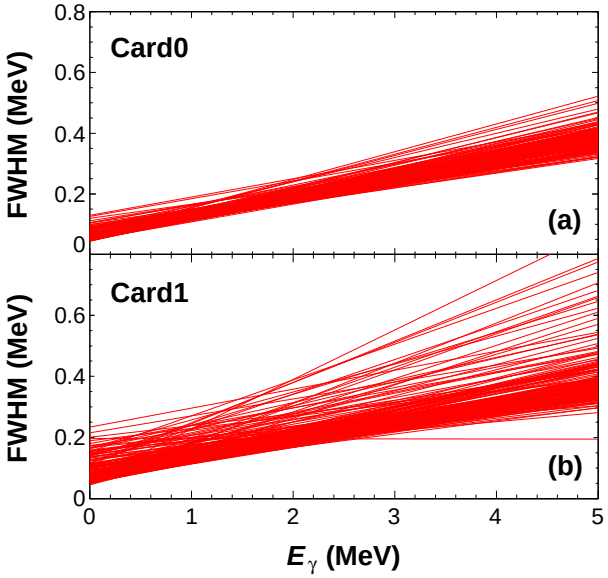

FIG. 3: Resolution of all DANCE detectors processed by digitizers of Card0 (a) and Card1 (b). The resolution was deduced from measurements with standard γ-rays sources and fitted with a line.

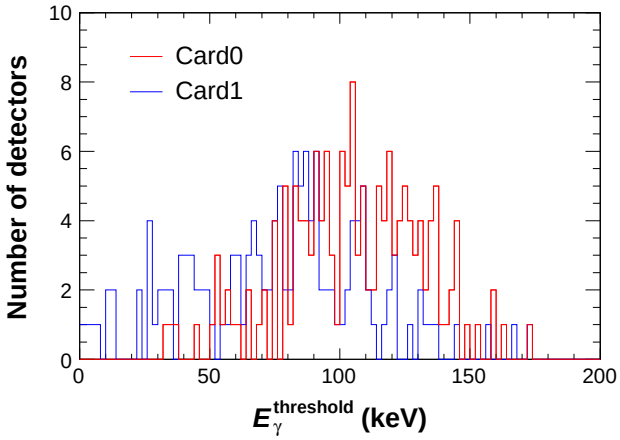

FIG. 4: Histograms of the threshold energies for all DANCE detectors. The thresholds were obtained by fitting the beginning of histograms from source measurements with a Gaussian function.

chosen as a superposition of a linear and a step function. Example spectra from detector 0 are given in Fig. 2. The energy calibration was obtained as a liner fit of the five data points (*cf.* Fig. 2).

The spectra of α particles are useful tool for monitoring the photomultiplier-tube gain stability on a run-by-run basis. Examples of gain instability can be found in Ref. [1]. We collect α spectra from each DANCE detector and for each data file. The replay program fits the spectra with a pre-defined shape and compares the results with those from a reference measurement. The energy calibration is corrected (gain matching) if an offset of the position of the α peaks is observed. The reference spectra are collected from the replay of the measurements with standard γ-ray sources, because for them the energy calibration is accurately known.

After calibrating the detectors, we replayed the same source measurements and collected calibrated γ-ray spectra. These spectra were used to deduce the energy resolution and the threshold for each DANCE detector. This information is needed for performing more accurate detector-response simulations. The same five peaks were fitted with the same function described above. The full-width-at-half-maximum (FWHM) vs. E_γ dependence was approximated with a linear function. The resolution of the DANCE detectors is given in Fig. 3 for each of the two sets of digitizers Card0 and Card1.

The rising slope in the beginning of the spectra from measurements with ^{22}Na, ^{137}Cs, and ^{88}Y γ-ray sources was fitted with a Gaussian function without a background. The values for the mean and the dispersion of the Gaussian curve were averaged. Note, the dispersion of the threshold is larger than the energy resolution of the detector, because the leading edge discriminator introduces additional spread. The threshold of each detector was calculated as the γ-ray energy at 50% of the height of the Gaussian curve. We show in Fig. 4 histograms of the thresholds for the two sets of digitizers for all DANCE detectors.

Due to small differences in the length of the detector cables, there is a slight offset in TOF between any pair of detectors. We perform alignment in time of the detectors by collecting time-offset histograms of each DANCE detector i relative to detector 0, *i.e.* $\Delta t_i = \text{TOF}_i - \text{TOF}_0$. We determine the mean value of the Δt_i distribution and correct detector i for the time offset. Indeed, the statistic in these histograms is sufficient to perform the time-correction procedure on a run-by-run basis. A routine was embedded in the data-replay code and performs the time correction after reading a data file (*cf.* Ref. [7]). No second replay of the data is required. Figure 5 gives the time difference of the DANCE detectors and detector 0 for the ^{22}Na measurement and Card0 after the time correction was applied. It is apparent from Fig. 5 that a time coincidence window of $\Delta_t = \pm 5$ ns will include the majority of the events. A narrow coincidence window is desirable to reduce the accidental background. The $^{191}\text{Ir}(n,\gamma)$ data were analyzed using $\Delta_t = \pm 5 = 10$ ns coincidence window.

V. BACKGROUND REDUCTION

The background in measurements with DANCE is discussed in a number of publications, *e.g.* Refs. [12, 14, 15]. Here we will describe the background corrections applied to the $^{191}\text{Ir}(n,\gamma)$ data.

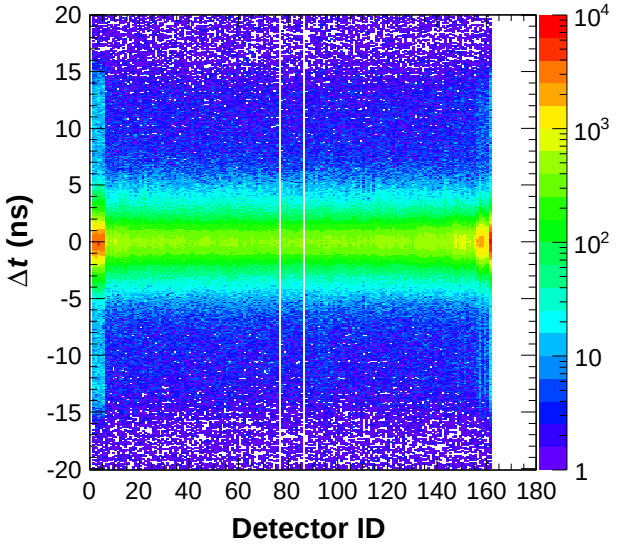

FIG. 5: Time difference Δ_t between each DANCE detector and detector 0 after the small time offsets between the detectors were corrected. The two blank vertical lines correspond to detectors removed for the beam line.

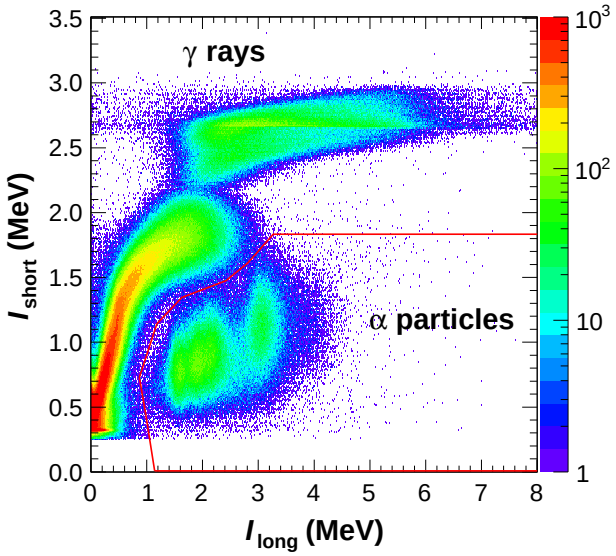

FIG. 6: Pulse-shape discrimination plot for detector 0 Card0 showing regions of α-particle and γ-ray events. A cut is drawn in red to remove the signals from the α particles.

A. Time-independent background

The natural γ-ray activity, like ^{40}K (1460.8 keV) and ^{208}Tl (2614.5 keV), is one source of time-independent background. It is easily removed by applying a E_γ^{tot} cut at the Q-value of the ^{191}Ir(n,γ) of 6.2 MeV. The high altitude of LANSCE causes a strong cosmic-rays background, like γ-ray showers and neutrons that can be captured in the structural material of the experimental hall. An E_γ^{tot} cut cannot remove this background, because the γ-ray energies vary in a wide range. We remove the cosmic-rays background when subtracting the measurement with ^{208}Pb from the ^{191}Ir data, see below.

The BaF_2 crystals contain a small (0.2 Bq/cm^3 [5]) contamination of radium, because barium and radium are chemical homologues. The α decay of the ^{226}Ra chain causes the observation of four strong peaks in the measured spectra. The BaF_2 detectors exhibit pulse-shape discrimination properties that allow removal of the α signals. A plot of I_{short} vs. I_{long} for detector 0 is shown in Fig. 6 with a cut removing the α signals. Such cuts have been drawn for each of the 2×160 detectors, because the position of the α peaks may vary from detector to detector. Because the waveform integral I_{long} provides the energy of the detected γ ray, we perform the energy calibration and the α-signals removal in a lengthy iterative way. First, we calibrate the DANCE detectors without α cuts applied and replay the source measurement to obtain the I_{short} vs. I_{long} plots in MeV. Then we draw the α cuts and replay the source measurements to produce for each detector a γ-ray spectrum without the α peaks. We again calibrate the detectors, replay the source measurements and correct the α cuts. We repeat this procedure for a third time to make sure the α cuts do not remove any γ rays.

B. Time-dependent background

The neutron beam is accompanied by γ rays produced by the spallation target. This background is related to the time structure of the proton beam, but is very small in magnitude due to the shielding of DANCE and having the last window of the flight-path collimator made out of Kapton [14]. Contribution of this background will be removed by subtraction of the ^{208}Pb measurement from the ^{191}Ir data.

The BaF_2 scintillators have a long component of the emitted light (*c.f.* section II). Single-photon de-excitations in the crystal may cause the DAQ to trigger again and consider the tail of the signal as a new γ ray. This effect we call re-triggering. It results in double counting of a γ ray. Even worse, if an α particle is detected, the re-triggering event shows as a γ ray in the I_{short} vs. I_{long} plot (*c.f.* Fig. 6). To remove the re-triggering events, we plot the ratio of the integrals I_{long} for two consecutive events i and $i+1$ for each detector as a function of the time difference TOF$_{i+1}$-TOF$_i$ between the events. Figure 7 shows such a plot for detector 0. The re-triggering events appear in the bottom left corner. A simple rejection condition of (TOF$_{i+1}$ - TOF$_i$) < 10 μs is not a good option, because we will lose many real events. Therefore, we drew a cut around the re-triggering events (*cf.* Fig. 7) to remove them during the replay of the data. Such cuts were drawn for all 2×160 detectors, because of the slight differences between them.

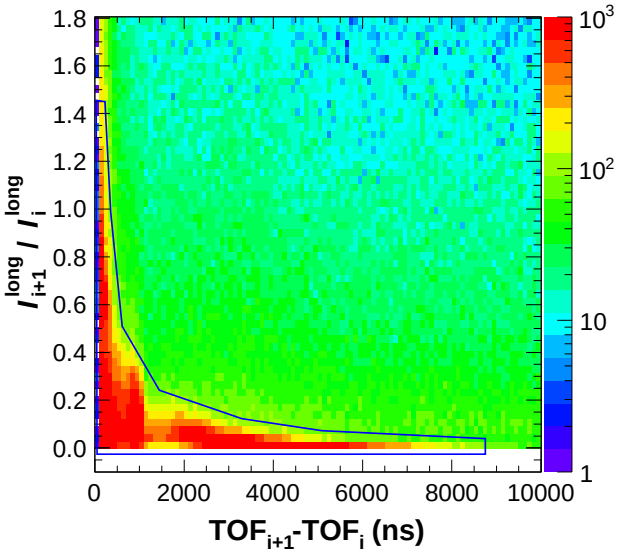

FIG. 7: Plot of ratios of the I_{long} integrals for two consecutive events in a detector vs. the time difference between them showing events due to re-triggering in the bottom left corner. A cut in blue is drawn to remove the re-triggering events.

C. Sample-related background

The target causes scattering of beam neutrons toward DANCE. These scattered neutrons are source of sample-related background. They may be captured in the structural material of DANCE and the detectors. DANCE is equipped with a ^{6}LiH shell with thickness of 6 cm surrounding the target that absorbs most of the scattered neutrons. Neutrons can be captured by the barium isotopes in the BaF_2 detectors and produce peaks in the E_γ^{tot} spectrum. The Q values of the (n,γ) reactions are Q = 9.108 MeV for ^{135}Ba(n,γ) (6.6% natural abundance), Q = 6.906 MeV for ^{136}Ba(n,γ) (n.a. 7.9%), Q = 8.612 MeV for ^{137}Ba(n,γ) (n.a. 11.2%), and Q = 4.723 MeV for ^{138}Ba(n,γ) (n.a. 71.7%).

Measurements with a ^{208}Pb target have been performed to measure the sample-related background (*c.f.* Table III). A comparison of E_γ^{tot} spectra measured with the 16-mg ^{191}Ir target and the ^{208}Pb target normalized to the neutron fluence is shown in Fig. 8. The comparison for $E_\gamma^{tot} > 10$ MeV shows that the ^{208}Pb measurement approximates well the background from cosmic rays. The ratio of the integrals of the two spectra between 12 and 20 MeV is 1.027. We will use this factor to scale the TOF spectrum from the measurements with ^{208}Pb target in section VII when subtracting it from the ^{191}Ir TOF spectra.

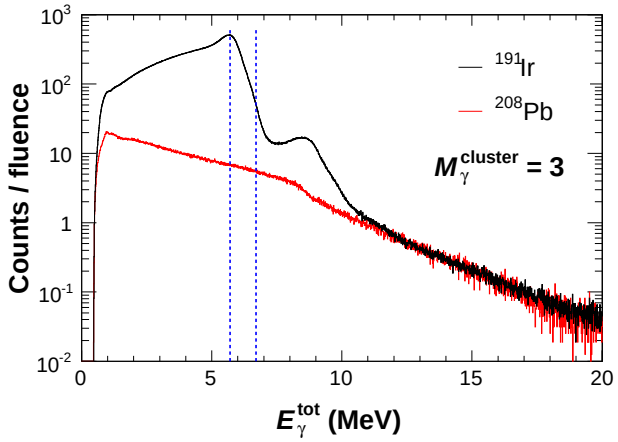

FIG. 8: E_γ^{tot} spectra from measurements with ^{191}Ir and ^{208}Pb targets normalized to their neutron fluences. The E_γ^{tot} spectra were collected for γ-ray multiplicity $M_\gamma = 3$. The vertical blue lines depict the E_γ^{tot} cut of 6.2 ± 0.5 MeV corresponding to the Q-value of the ^{191}Ir(n,γ) reaction.

VI. NEUTRON FLUENCE

DANCE is equipped with three neutron detectors to monitor the neutron beam. The beam monitors are located downstream of DANCE in the following order: a ^{6}Li monitor, a ^{3}He monitor, and a ^{235}U fission chamber. Details about the beam detectors can be found in Ref. [12]. The quantity of interest is the neutron fluence (neutron flux $\times$ time of the measurement), because it gives us normalization when combining all ^{191}Ir measurements together.

The ^{6}Li monitor consists of a 2-μm thick ^{6}LiF target and a surface barrier Si detector. The target is tilted at 45° relative to the beam and the Si detector is at 90° relative to the beam. The ^{6}LiF target is located at 22.59 m from the neutron moderator. The monitor detects neutrons through the reaction ^{6}Li$(n,t)^4$He. The Si detector measures both the tritons and the α particles produced by the reactions. We drew a cut in a I_{short} vs. I_{long} plot to collect a spectrum of the tritons only. The tritons spectrum from all ^{191}Ir measurements with the 16 mg target, the cross section for the ^{6}Li$(n,t)^4$He reaction [16] and the deduced neutron fluence are shown in Fig. 9. The integral of the fluence spectrum from the ^{6}Li monitor for each of the ^{191}Ir measurements is given in Tables I and II. The dips in the spectrum above E_n = 10 keV are due to absorption of neutrons in the aluminum windows of the neutron-production target and of the different sections of the neutron-beam collimator.

The second neutron monitor is a ^{3}He counter with a ^{3}He areal density of 1.882×10^{17} atoms/cm^2. It detects neutrons via the ^{3}He$(n,p)^3$H reaction. The monitor is positioned at 22.76 m from the neutron moderator. We drew a cut in a I_{short} vs. I_{long} plot to collect a spectrum of the protons only. We calculate the neutron spectrum knowing the cross section for the ^{3}He$(n,p)^3$H reaction

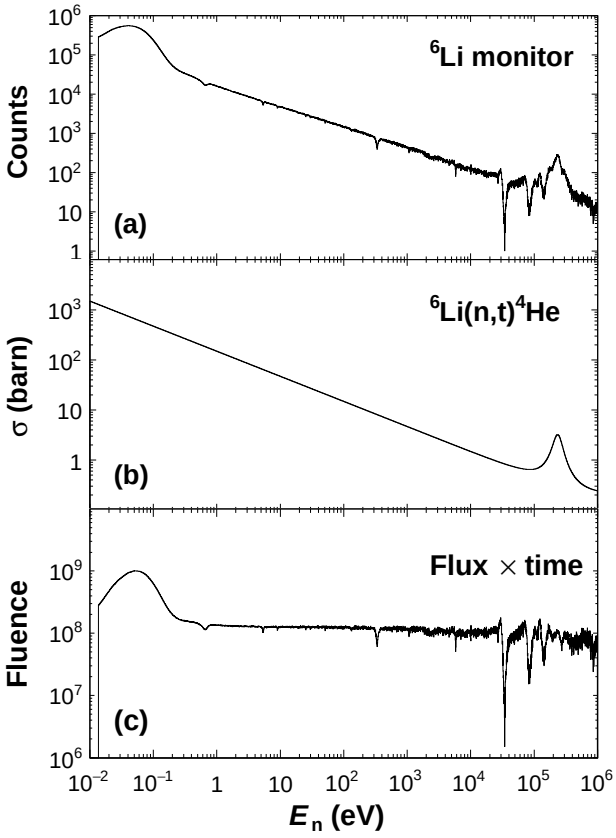

FIG. 9: A spectrum of tritons (a) measured from the ^{6}Li$(n,t)^4$He reaction with a Si detector. The cross section (b) for the reaction from [16] and the deduced neutron fluence (c). The dips in the spectrum above $E_n = 10$ keV are due to absorption of neutrons in the aluminum windows installed along the beam line.

[16].

The last neutron monitor is a ^{235}U fission chamber filled with P-10 gas and containing a ^{235}U target with thickness of 1.3 mg/cm^2 and diameter of 6.99 cm. The monitor is located at 22.82 m from the neutron moderator. Only one of the fission fragments produced a signal because of the thick backing of the target. We calculated the neutron fluence using the ^{235}U(n,f) cross section [16].

A comparison of the neutron fluence from the three monitors is shown in Fig. 10. The spikes in the spectrum from the ^{235}U monitor are due to the neutron-beam resolution in the resonance region. The spectrum from the ^{3}He monitor had to be cut above 60 keV because of high noise. Overall the three monitors show the same shape of the neutron flux.

VII. RELATIVE CROSS SECTION

We obtained the TOF spectra from all individual measurements applying a Q-value cut from 5.7 to 6.7 MeV

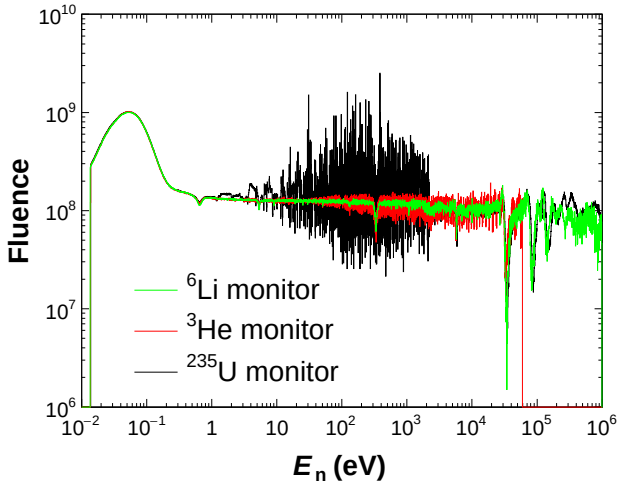

FIG. 10: Comparison of the neutron fluence obtained from the three neutron-beam monitors showing a consistent shape of the neutron-flux spectrum. The spikes in the ^{235}U monitor are due to the neutron-beam resolution.

and requiring a γ-ray multiplicity $M_\gamma \geq 3$ to reduce the natural background. Note, the Q value for the ^{191}Ir(n,γ) reaction is 6.198 MeV. We combined the TOF spectra from all measurements with the 16 mg target. The TOF spectra were corrected for the neutron fluence taken from Table II. The TOF spectrum converted to neutron energy with binning of 1000 bins/decade is shown in Fig. 11. We trimmed the beginning and the end of the individual spectra to avoid overlaps between them and, respectively, bumps in the sum spectrum. A gap was produced at $E_n = 37$ eV due to the exact offset of 250μs set for the second digitizer card. A measurement (runs 43919-43934) was performed with the goal to fill this gap, we used only a few bins from it shown in yellow in Fig. 11.

We replayed the measurements with the ^{208}Pb target (*cf.* Table III) using the same conditions as for ^{191}Ir to obtain the background due to neutrons scattered from the ^{191}Ir target. The background spectrum is shown in red in Fig. 11. It was scaled by a factor of 1.027 obtained in section V (*cf.* Fig. 8).

For completeness, we produced the same combined TOF from the measurements with the thin electroplated ^{191}Ir target (not shown). This spectrum was not useful for extracting the (n,γ) cross section, because of the small statistics of the individual measurements and missing data. For unknown reason the digitizers from Card1 stopped producing data for most of the measurements listed in Table I. A third reason for abandoning the measurements with the thin target is that the individual TOF spectra do not merge well after correction for the neutron fluence. The combined spectrum shown jumps in contrast with Fig. 11.

We calculated the relative cross section by first subtracting the background spectrum from the combined TOF spectrum and then dividing the residuum spectrum

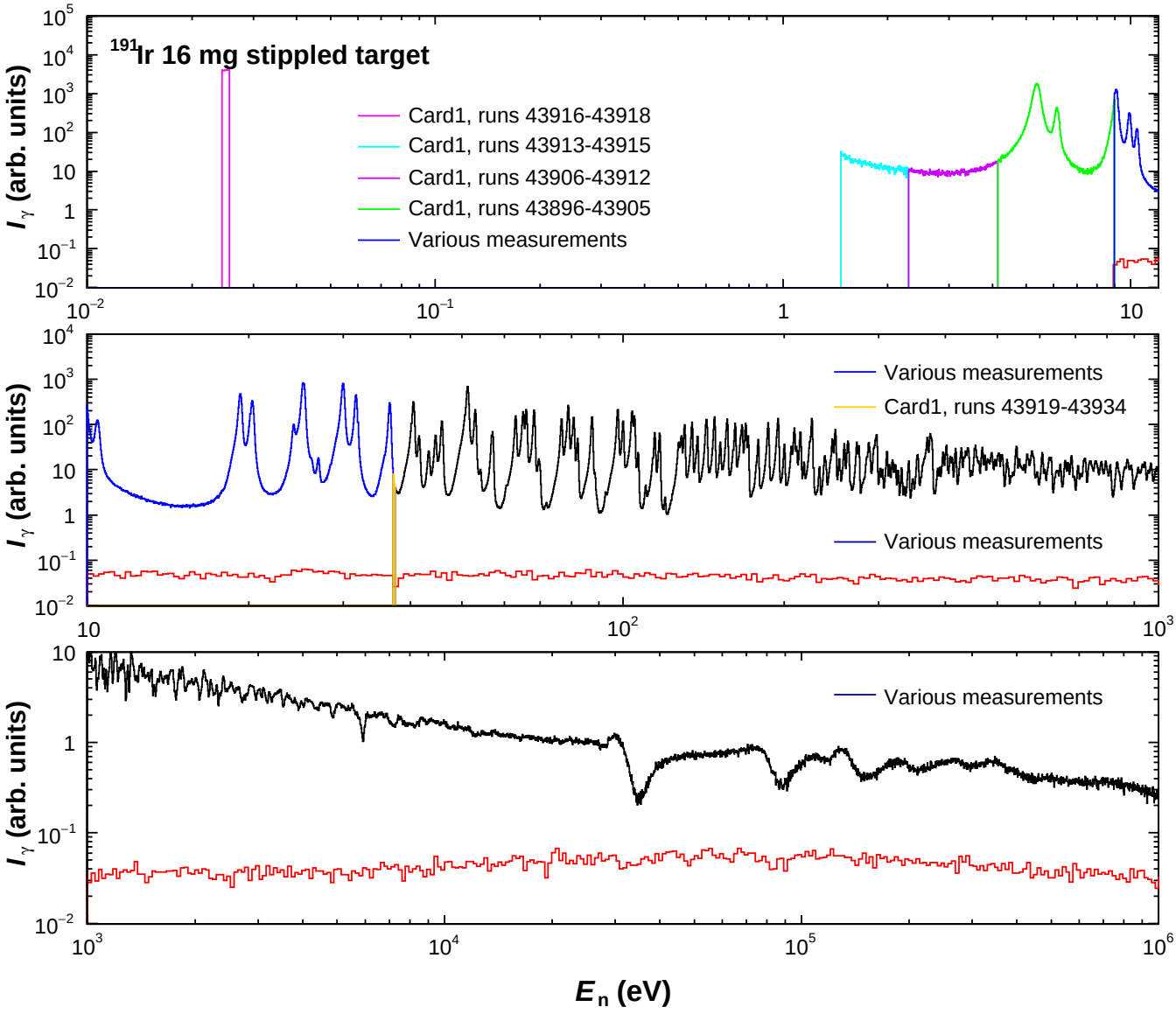

FIG. 11: Time-of-flight spectrum, converted to neutron energy, from all individual measurements with the thick ^{191}Ir target normalized by their neutron fluences given in Table 11. The run numbers of the measurements are given in the legend. For some of the measurements the delay of the 250 μs window was the same and the spectra were added up and labeled as "various measurements." The background spectrum obtained from the measurements with ^{208}Pb target is shown in red.

by the neutron flux from the ^{6}Li monitor (*cf.* Fig. 9(c)). The background does not extend below $E_n = 9$ eV, but this is not critical for obtaining the relative cross section at lower energies, because the contribution of the background is negligible. We normalized the relative cross section to the absolute one from the ENDF/B-VIII.0 [16] at 0.025 eV by integrating the spectrum shown in pink in Fig. 11. The obtained cross section from the DANCE measurement compared to the ENDF evaluation is shown in Fig. 12. The peaks above $E_n = 30$ keV are artificial due to the dips in the neutron flux and have to be ignored. The uncertainty propagation includes only the statistical uncertainties from the TOF spectra, the background spectrum, the neutron flux spectrum, and the integral of the individual neutron-fluence spectra given in Table II.

Closer examination of the comparison with the ENDF cross section reveals small resonances that present only in the DANCE data. Because the Q values for the ^{191}Ir(n,γ) and the ^{193}Ir(n,γ) are close, 6.198 and 6.067 MeV, respectively, small amount of ^{193}Ir in the target can cause observation of ^{193}Ir(n,γ) resonances. These extra resonances will be removed in a resonances analysis using the data from Ref. [1].

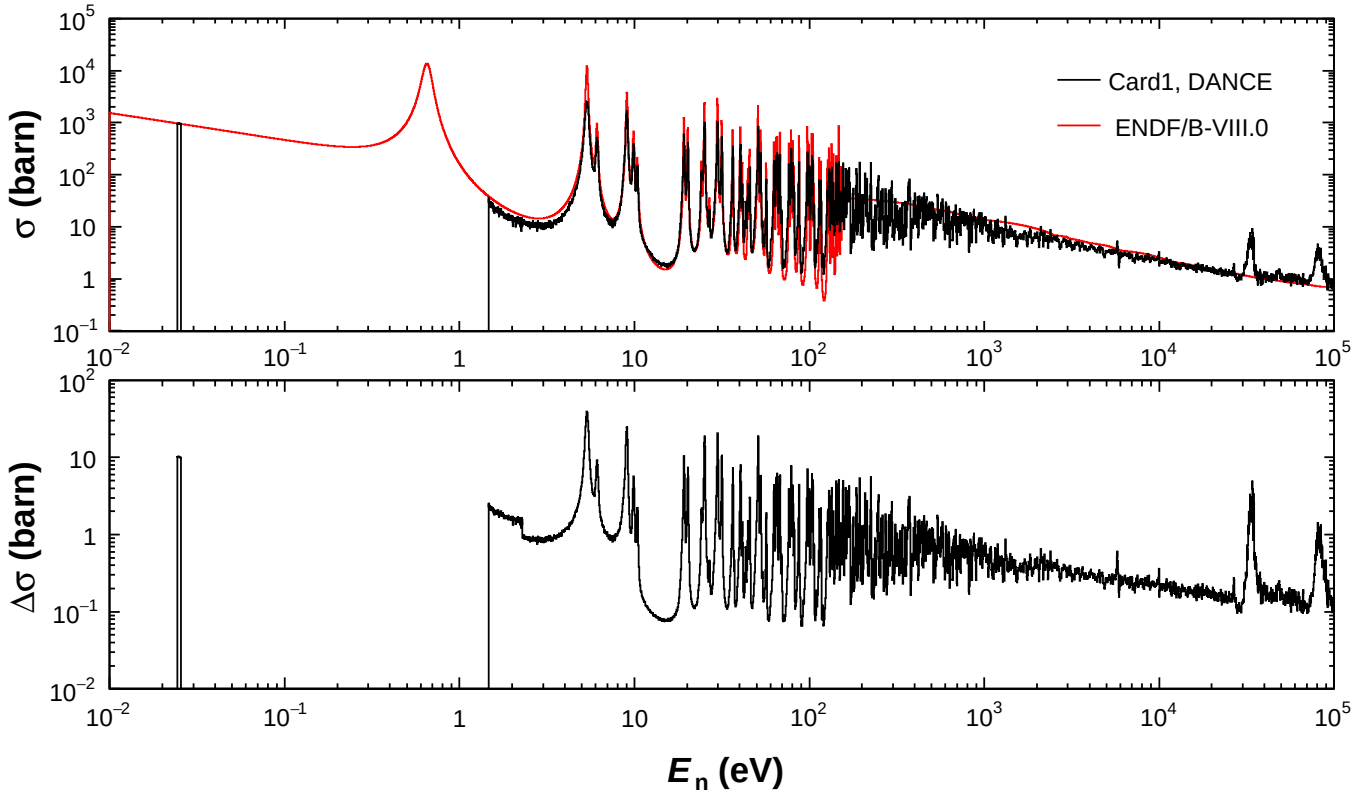

FIG. 12: Relative cross section for the ^{191}Ir(n,γ) reaction obtained from this work (upper panel). The cross section is normalized to the one from the ENDF evaluation at $E_n = 0.025$ eV. The peaks above $E_n = 30$ keV are artificial and have to be ignored. The uncertainty propagation is shown on the bottom panel and is based only on the statistical uncertainty of the measured spectra with DANCE and the ^{6}Li monitor.

VIII. SUMMARY

Analysis of former DANCE data from the ^{191}Ir(n,γ) reaction with a thick target was performed and relative neutron-capture cross section obtained above 1 eV. A second set of measurements with a thin ^{191}Ir target was irnored, because of small statisctics and DAQ malfunctioning. Resonance analysis is required to extract the parameters of resonances above $E_n = 150$ eV and to remove weak resonances from the ^{193}Ir(n,γ) reaction. Only staistical uncertainties were considered. Transport-code simulations are needed to estimate the systematic uncertainties.

A new advanced DAQ of DANCE is in opperation since 2016 [7]. It provides a complete TOF spectrum and does not suffer from the 250-μs TOF window limitation of the old Acqiris digitizers. Repeating the ^{191}Ir(n,γ) measurement at DANCE will be beneficial. It will provide the neutron-capture cross section from the thermal region to 1 MeV.

Acknowledgments

This work was performed under the auspices of the National Nuclear Security Administration of the U.S. Department of Energy at Los Alamos National Laboratory under Contract DE-AC52-06NA25396.

[1] M. Jandel, C. W. Arnold, B. Baramsai, T. A. Bredeweg, E. M. Bond, A. Couture, R. C. Haight, M. Mocko, R. S. Rundberg, G. Rusev, et al., LANL report **LA-UR-15-27342** (2015).
[2] P. W. Lisowski and K. F. Schoenberg, Nucl. Instrum. Methods A **562**, 910 (2006).
[3] M. Mocko, G. Muhrer, F. Tovesson, and J. Ullmann, *Proceedings of the International Topical Meeting on Nuclear Research Applications and Utilization of Accelerators*, Vienna, May 4-8, **AP/IE-03** (2009).
[4] M. Mocko and G. Muhrer, Nucl. Instrum. Methods A **704**, 27 (2013).
[5] M. Heil, R. Reifarth, M. M. Fowler, R. C. Haight, F. Käppeler, R. S. Rundberg, E. H. Seabury, J. L. Ullmann, J. B. Wilhelmy, and K. Wisshak, Nucl. Instrum. Methods A **459**, 229 (2001).
[6] M. Jandel, T. A. Bredeweg, A. Couture, M. M. Fowler, E. M. Bond, M. B. Chadwick, R. R. C.

Clement, E.-I. Esch, J. M. ODonnell, R. Reifarth, et al., Nucl. Instrum. Methods B **261**, 1117 (2007).
[7] M. Jandel, B. Baramsai, T. A. Bredeweg, A. Couture, A. Favalli, A. C. Hayes, K. D. Ianakiev, M. L. Iliev, T. Kawano, S. Mosby, et al., Nucl. Instrum. Methods A **882**, 105 (2018).
[8] R. Y. Zhu, J. Phys. Conf. Series **587**, 0.12055 (2015).
[9] J. M. Wouters, A. A. Vicente, T. A. Bredeweg, E. Esch, R. C. Haight, R. Hatarik, J. M. O'Donnell, R. Reifarth, R. S. Rundberg, J. M. Schwantes, et al., IEEE Trans. Nucl. Sci. **53**, 880 (2006).
[10] URL `https://midas.psi.ch/`.
[11] E. M. Bond, W. A. Moody, C. Arnold, T. A. Bredeweg, M. Jandel, and G. Y. Rusev, J. Rad. Nucl. Chem. **307**, 1981 (2016).
[12] M. Jandel, T. A. Bredeweg, E. M. Bond, M. B. Chadwick, R. R. Clement, A. Couture, J. M. O'Donnell, R. C. Haight, T. Kawano, R. Reifarth, et al., Phys. Rev. C **78**, 034609 (2008).
[13] M. Jandel, T. A. Bredeweg, A. Couture, J. M. O'Donnell, and J. L. Ullmann, LANL technical report **LA-UR-12-21171** (2012).
[14] R. Reifarth, T. A. Bredeweg, A. Alpizar-Vicente, J. C. Browne, E.-I. Esch, U. Greife, R. C. Haight, R. Hatarik, A. Kronenberg, J. M. O'Donnell, et al., Nucl. Instrum. Methods A **531**, 530 (2004).
[15] E.-I. Esch, R. Reifarth, E. M. Bond, T. A. Bredeweg, A. Couture, S. E. Glover, U. Greife, R. C. Haight, A. M. Hatarik, R. Hatarik, et al., Phys. Rev. C **77**, 034309 (2008).
[16] *ENDF/B-VIII.0 evaluation*, URL `http://www.nndc.bnl.gov/exfor/endf00.jsp/`.